Clays and Clay Minerals, Vol. 69, No. 6:672–687, 2021

MEIFUITE, A NEW FERROUS PHYLLOSILICATE MINERAL WITH MODULATED TETRAHEDRAL SHEETS SIMILAR TO MINNESOTAITE

Shiyun Jin[1], Xiaochun Li[2,3]*, Franklin Hobbs[1], Stephen Guggenheim[4], and And Huifang Xu[1]*

[1]S. W. Bailey X-ray Diffraction Laboratory, Department of Geoscience, University of Wisconsin–Madison, Madison, WI 53706, USA
[2]Key Laboratory of Mineral Resources, Institute of Geology and Geophysics, Chinese Academy of Sciences, Beijing 100029, China
[3]College of Earth and Planetary Sciences, University of Chinese Academy of Sciences, Beijing 100049, China
[4]Department of Earth and Environmental Sciences, University of Illinois at Chicago, Chicago, IL 60607, USA

Abstract—A new ferrous phyllosilicate, meifuite, has been discovered in the Yinachang Fe-Cu-REE (rare-earth element) deposit in China. The structural formula, calculated using averaged electron probe microanalysis (EPMA) results, is $K_{0.72}Na_{0.20}(Fe_{5.56}Mg_{0.31}Mn_{0.13})_{\Sigma 6.00}(Si_{6.95}Al_{1.04})_{\Sigma 7.99}O_{18.84}(OH)_{4.84}Cl_{1.33}$, with an ideal formula of $KFe_6(AlSi_7)O_{19}(OH)_4Cl_2$. The structure of meifuite has a $P\bar{1}$ space group symmetry, with unit-cell parameters of a = 22.7773(13) Å, b = 9.5553(5) Å, c =14.3282(8) Å, α = 99.258(4)°, β = 136.750(3)°, γ = 89.899(4)°, Z = 2, and V = 2077.9(2) Å^3. Meifuite has a strip-modulated 2:1 layer (T–O–T) structure similar to that of minnesotaite. About 1/8 of the tetrahedra in the T sheet are occupied by Al instead of Si, and the interlayer cavities are partially occupied by K and Na. Some of the OH sites in the octahedral sheet in the layer structure are fully or partially substituted by Cl, which is apparently the primary reason for the meifuite structure being more stable than stilpnomelane, the most common ferrous layer silicate mineral found at similar temperature and pressure conditions. An updated, more accurate structure model of minnesotaite is also provided for comparison with the meifuite structure. The mineral is named after Meifu Zhou in honor of his outstanding contributions to the field of economic geology.

Keywords—Fe-silicate mineral · Meifuite · Single-crystal XRD · Strip modulated layer structure

INTRODUCTION

Phyllosilicates, or layer silicates, are an important group of minerals where the structures consist of 2-dimensional sheets of silicon tetrahedra generally sharing three corners with each other. Most phyllosilicates also contain continuous sheets of edge-sharing octahedra filled by larger cations such as Al, Mg, and Fe, which are connected to the unshared corners of the tetrahedra. Thus, the common phyllosilicate minerals are further categorized into 1:1 (T–O) and 2:1 (T–O–T) layers, based on the ratio between tetrahedral (T) and octahedral (O) sheets. Complicated structures of layer silicate minerals are often created when the size discrepancy between tetrahedral and octahedral sheets is too large and modifications are needed to match them together. Therefore, a large variety of such layered structures is found in nature, making the phyllosilicates one of the most diverse groups of minerals.

Ferrous phyllosilicate minerals are a significant and complex subgroup of the layer silicates, which are often found in iron-rich metamorphic systems, such as banded iron formations. Studying these mineral species and their relations to each other is critical to understand these complicated geological systems. The relatively large Fe(II) atoms cause a mismatch between the octahedral and tetrahedral sheets, making their structures more diverse compared to Mg- or Al-rich layer silicates (Guggenheim and Eggleton, 1987). Four ferrous phyllosilicate mineral species with 2:1 layer structures, annite, stilpnomelane, zussmanite, and minnesotaite, are commonly found in Fe-rich rocks. Annite is the Fe end member of the annite-phlogopite solid solution series, which has the common mica structure. In ideal annite, one quarter of the tetrahedra in the T sheet are occupied by Al instead of Si, expanding the tetrahedral sheet to match the Fe-filled octahedral sheet (Hazen & Burnham, 1973). Zussmanite and stilpnomelane have "island structures," where the tetrahedral sheet is separated into small islands of hexagonal ring(s), which are bridged by interlayer tetrahedra that are not connected directly to the octahedral sheets (Eggleton & Bailey, 1964; Lopes-Vieira & Zussman, 1969; Eggleton, 1972; Eggleton & Chappell, 1978; Guggenheim & Eggleton, 1994). The islands of hexagonal rings are larger in the structure of stilpnomelane (7 hexagons), and are bridged by a double hexagonal cage across adjacent sheets and layers. The islands in the zussmanite structure, in contrast, are smaller (single hexagon), and are bridged by a single tetrahedral triangle across adjacent sheets and layers. Stilpnomelane has a larger d_{001} value compared to the other 2:1 layer silicates due to the double hexagonal cages that bridge the layers, which allow the structure to accommodate interlayer cations and water molecules. Minnesotaite has a 'strip structure,' where strips of hexagonal rings parallel to the ***b*** axis are bridged with interlayer tetrahedral single chains. The width of an individual strip may vary

* E-mail address of corresponding author: hfxu@geology.wisc.edu
DOI: 10.1007/s42860-021-00143-8

depending on the Fe/Mg ratio in the octahedral sheet (Guggenheim & Bailey, 1982; Guggenheim & Eggleton, 1986b).

A new ferrous 2:1 layer phyllosilicate mineral, meifuite, was discovered recently in the Yinachang Fe-Cu-REE (rare-earth element) deposit in China. Meifuite has a similar strip structure to that found in minnesotaite, but some of the interlayer cavities are filled with cations, K and Na. The high-salinity hydrothermal fluid may be an important factor stabilizing the meifuite structure at temperature and pressure conditions similar to stilpnomelane. The details of appearance, physical properties, and crystal structure of meifuite are described here and relations with the other ferrous phyllosilicate are discussed. The newly discovered mineral is named after Prof. Mei-Fu Zhou (born in 1962) of the University of Hong Kong. Prof. Zhou has contributed significantly to the understanding of Proterozoic tectonic evolution and Fe-Cu metallogenesis of the Yangtze Block, South China. His research interests also include studies of ophiolites, large igneous provinces, and magmatic ore deposits. He has published >400 papers in scientific journals and several books. Prof. Zhou has been selected as fellow of the Geological Society of America (GSA) and serves as the Editor-in-Chief of the *Journal of Asian Earth Sciences*. The new mineral species and name have been approved by the Commission on New Minerals, Nomenclature and Classification (CNMNC) of the International Mineralogical Association (Jin et al., 2020, IMA 2019-101).

SAMPLE AND EXPERIMENTS

Meifuite was discovered in a Fe-Cu-REE ore deposit of the Yinachang, Yangtze Block, South China. The holotype specimen of meifuite (UWGM 6859) and two co-type specimens (UWGM 6860 and UWGM 6861) are stored permanently in the Geology Museum of the Department of Geoscience at the University of Wisconsin-Madison, USA. The Yinachang deposit was formed in a continental rift setting at ~1.7 Ga (Li et al., 2015). This deposit consists of several Fe-Cu-REE orebodies in Paleoproterozoic metasedimentary rocks (e.g. slate, schist, and dolostone). The Fe-Cu-REE ore was formed by the reaction of deeply derived, high-temperature, magmatic-hydrothermal fluids with meta-sedimentary rocks (Li et al., 2015). Low-temperature, non-magmatic fluids may also be involved in the ore-forming system, and facilitated metal precipitation.

Two main mineralization stages were identified in the Yinachang deposit, namely the Fe mineralization stage and Cu mineralization stage. In the Fe mineralization stage, hydrothermal minerals include mostly magnetite, siderite, and apatite; in the Cu mineralization stage, hydrothermal minerals include mostly chalcopyrite, ankerite, biotite, and fluorite. Meifuite was formed in the Fe mineralization stage, which commonly occurs in association with magnetite and siderite and is locally overprinted by chalcopyrite (Li et al., 2015). Fluid temperatures for the Fe-mineralization stage were estimated to range from ~400 to ~500°C, calculated from oxygen isotope thermometry on magnetite-siderite pairs (Li et al., 2015). The structures and mineral assemblage of the ore-hosting rocks suggest a relatively shallow and brittle environment under low pressure (Li et al., 2015).

Meifuite occurs as flaky or tabulate crystals 10–80 μm wide and 50–400 μm long, and appears to be very similar to muscovite. Optical microscopy images (plane-polarized, cross-polarized, and reflected light) of a thin section containing meifuite are shown in Fig. 1. Meifuite is almost always found in contact with siderite. Meifuite is nearly colorless with a slight pleochroic green color under plane polarized light. Larger crystals of meifuite are expected to be a darker greenish color when observed with the naked eye. Meifuite has an interference color of up to third-order green, with a birefringence of ~0.044. Meifuite is readily identified in backscattered-electron (BSE) images (Fig. 2) due to its elongated flaky shapes. Some basic physical properties of meifuite are listed in Table 1.

The chemical composition of the meifuite was analyzed with a CAMECA SX Five field emission electron probe at 15 kV and 10 nA beam current with a 5 μm beam size, using microcline, jadeite, augite, forsterite, tephroite, chlorapatite, and quartz as standards. H_2O is calculated by analysing the O by EPMA and assigning the excessive O to H_2O. The analysis resulted in an average chemical formula of $K_{0.72}Na_{0.20}(Fe_{5.56}Mg_{0.31}Mn_{0.13})_{\Sigma 6.00}(Si_{6.95}Al_{1.04})_{\Sigma 7.99}O_{18.84}(OH)_{4.84}Cl_{1.33}$. The results of the chemical analysis are listed in Table 2.

A Raman spectrum was measured using a high-resolution Raman spectrometer (LabRAM HR 800, Jobin-Yvon Horiba, Kyoto, Japan). The Raman spectrometer was equipped with a Si-based, charge-coupled device (CCD) detector, an integrated Olympus BX41 optical microscope, and an automatized *x-y* stage. Raman spectra were collected with a 532.21 nm (frequency-doubled Nd: YAG) laser excitation, a 50× long-distance objective with 0.55 numerical aperture, a 100 μm slit width, and a 1800 groove/mm grating. The corresponding spectral resolution was ~1 cm^{-1}. The spectra were acquired for an exposure time of 5 s with two accumulations. Spectra were calibrated using the 520.7 cm^{-1} peak of a silicon wafer. Data acquisition and spectra treatment were performed with the program *LabSpec5* (HORIBA Jobin Yvon GmbH, Bensheim, Germany). The Raman spectroscopy result is shown in Fig. 3.

Crystals were cut from petrographic thin sections for single-crystal X-ray diffraction analysis. X-ray diffraction data were collected on a Bruker Quazar APEXII single-crystal diffractometer with a MoKα IμS source and APEX2 detector. The instrument was run at a voltage of 50 kV and current of 0.6 mA. Unit-cell parameters were calculated and refined using *APEX3* software. The refinement of the structures was performed with *JANA2006* software (Petříček et al., 2014) on F^2. The 3D crystal structure was visualized by *VESTA* (Momma & Izumi, 2011). The experimental and crystallographic information are listed in Table 3.

A corrected structure model for minnesotaite, based on the structure of meifuite, has also been proposed here for comparison. First-principles calculations of the corrected minnesotaite structure

https://doi.org/10.1007/s42860-021-00143-8 Published online by Cambridge University Press

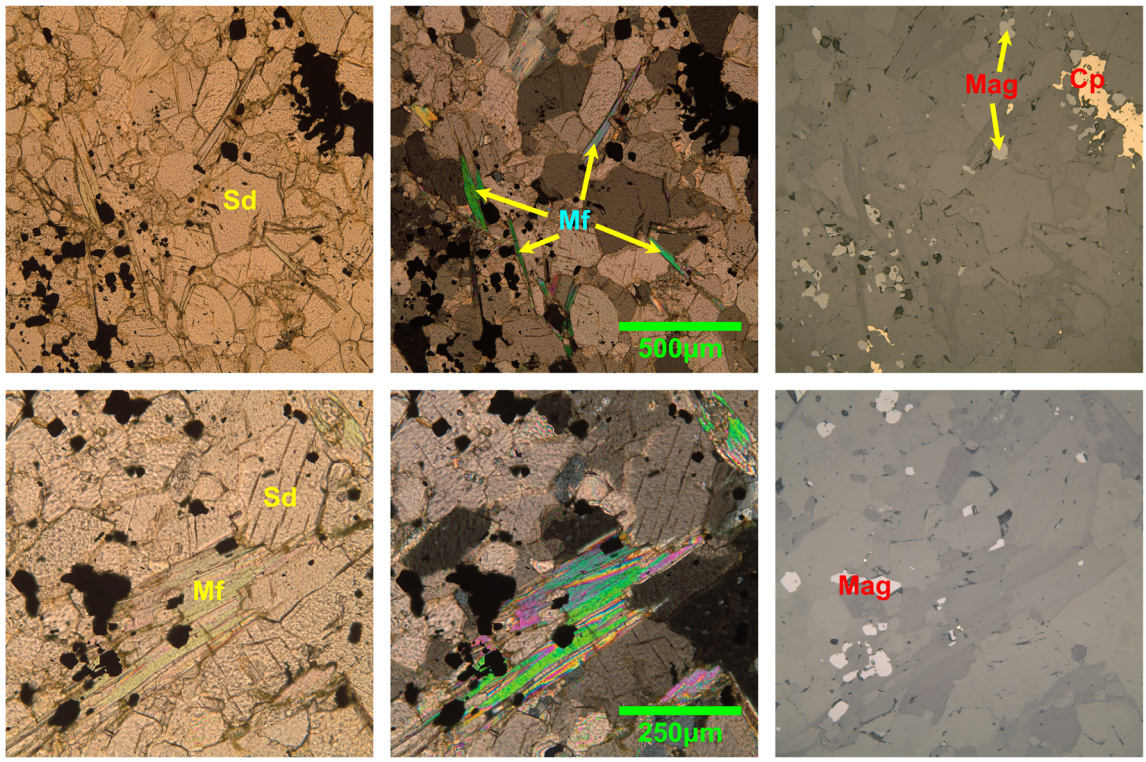

Fig. 1 Optical microscopy images of meifuite in thin section, under plane polarized light (left), cross polarized light (middle), and reflected light (right).The meifuite crystals are often found in contact with siderite and magnetite. (Mf: meifuite; Sd: siderite, Cp: chalcopyrite; Mag: magnetite)

were performed with the Vienna *Ab initio* Simulation Package (VASP) using projector augmented wave pseudopotentials and the general gradient approximation (GGA) with Perdew, Burke, and Ernzerhof parameters (Blöchl, 1994; Kresse & Furthmülller, 1996; Perdew et al., 1996; Kresse & Joubert, 1999). All calculations used a 600 eV energy cut-off with a 1×3×3 k-point mesh. Gaussian smearing was used with a sigma value of 0.05 eV. Local energy minima were found using the conjugate gradient algorithm and atomic positions were allowed to relax within a fixed cell constant. An additional Hubbard-type term of 4.0 eV was applied to the iron in the GGA+U method (Wang et al., 2006). Partial occupancies were not considered and the initial structure was based on an $Fe_{30}Si_{40}O_{96}(OH)_{28}$ structure with a = 28.4716 Å, b = 9.5553 Å, c = 12.4087 Å, α = 100.682°, β = 127.705°, γ = 89.899° (following the lattice parameters of meifuite). A fully relaxed box was also considered and resulted in a 3–5% reduction in the unit-cell parameters and a <0.2% change in unit-cell angles. The modulation orientations were maintained for both the fixed and relaxed unit cells (see the meifuite-minnesotaite.cif file in the Supplementary Material).

CRYSTAL STRUCTURE OF MEIFUITE

The meifuite structure has a primitive triclinic unit cell with a = 22.7773(13) Å, b = 9.5553(5) Å, c = 14.3282(8) Å, α = 99.258(4)°, β = 136.750(3)°, γ = 89.899(4)°, Z = 2, and V = 2077.9(2) Å^3, with a space group symmetry of $P\bar{1}$. The unit-cell setting was selected following the convention of layer silicate structures, with a and b axes perpendicular (pseudohexagonal cell) to each other within the octahedral sheet. Comparing the unit cell of meifuite with a 1*M* mica, the relation is $a_{mf} = 4a_{mic}$ and $b_{mf} = b_{mic}$, where the *C*-center symmetry is lost in meifuite due to the modulated tetrahedral sheet. The c axis of meifuite was selected to have the smallest α and β angles that are greater than >90°.

The structure solution and refinement of meifuite was straightforward. A structure solution could be reached easily using the charge-flipping method, with Fe, Si, and K assigned to the octahedral sites, tetrahedral sites, and interlayer sites, respectively, and O assigned to all the anion sites. A Fourier difference map was constructed after the initial convergence to assess the structure, where the most obvious electron density peaks appeared near some oxygen atoms on the O-sheet, which corresponded to the Cl atoms. The corresponding anions were split into disordered Cl and O atoms with total occupancy constrained to 1, except for two anion sites where all the electron density appears at the Cl position. The occupancies of all the cations were relaxed in the following refinement. Mg was added to octahedral sites of which the Fe occupancy was significantly <1, the rest of the octahedral sites were restored to fully occupied by Fe. The average T–O distances were calculated for all the tetrahedra in the structure, and the two largest T sites were assigned with Al instead of Si. Na was added to the interlayer sites A_1 and A_2, with the position and atomic displacement parameters (ADPs) constrained to the same for K and Na in each site, and total occupancy of A_1 and A_2

https://doi.org/10.1007/s42860-021-00143-8 Published online by Cambridge University Press

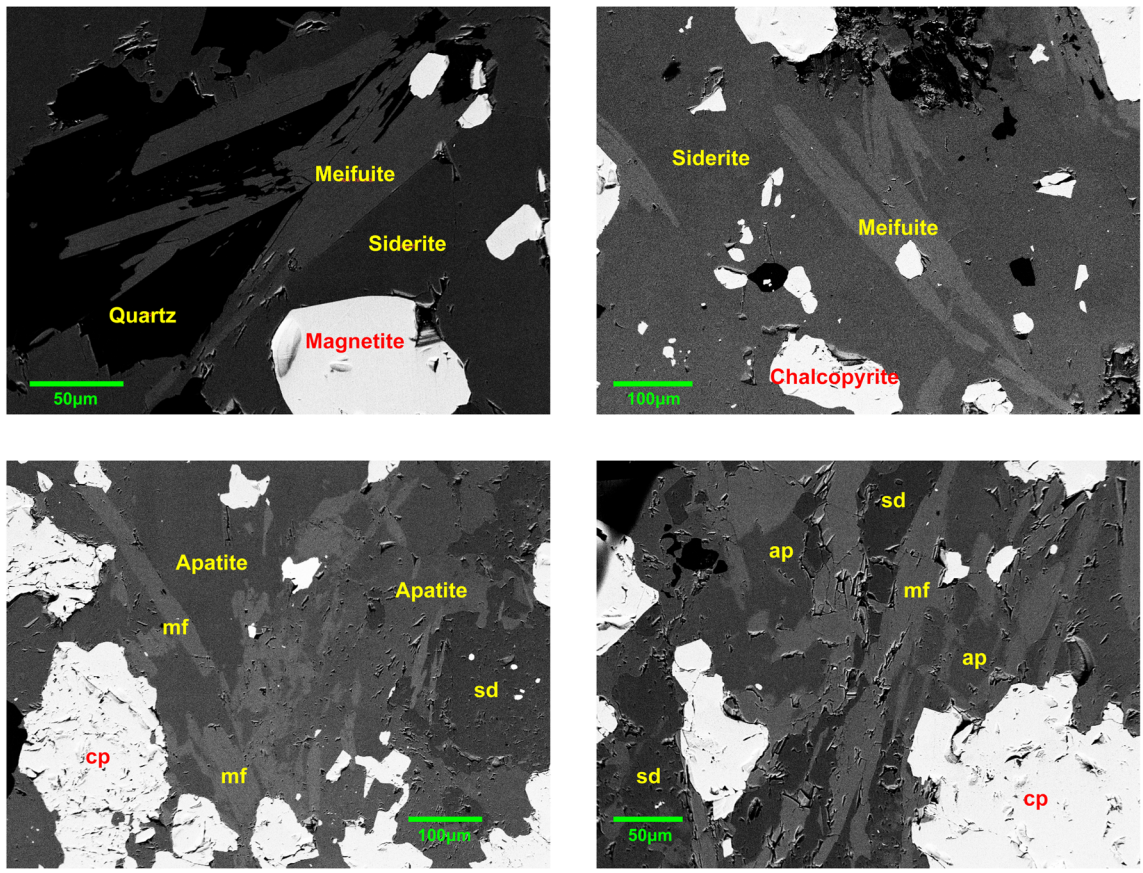

Fig. 2 Back-scattered electron (BSE) images of meifuite in thin section. Meifuite crystals are readily identified from the flaky crystal shape. Meifuite appears slightly brighter than apatite and siderite in the BSE images. Meifuite crystals are also in contact with apatite and quartz

constrained to 0.85 and 0.7, respectively, based on the relative K occupancy, which resulted in a similar K/Na ratio as the chemical analysis result. The isotropic ADPs were then relaxed to harmonic ADPs for every atom in the structure, which resulted in many atoms having non-positive, definite ADPs. The atoms with realistic displacement parameters all showed thermal ellipsoids with similar orientation and amplitude. Therefore, all the atoms with non-positive definite ADPs were fixed to have the same ADPs with the other atoms of the same type. The atomic positions in the structure of meifuite are listed in Table 4, and the bond distances in the structure are listed in Table 5.

The crystal structure of meifuite, projected along several different directions, is illustrated in Fig. 4. The structure has a continuous trioctahedral sheet (O-sheet) filled with Fe(II) sandwiched by two tetrahedral sheets (T-sheet). The T-sheets are not a continuous 2D tetrahedral network constructed only by six-membered rings, as in common layer silicates such as talc. Instead, the T-sheets are modulated by single chains that connect two adjacent 2:1 layers. Between these interlayer single chains, the tetrahedra are connected to the O-sheet similar to the 2D hexagonal network found in common layer silicates. Because the modulation occurs along the *a* axis, the tetrahedra form rows (spatially aligned but not necessarily connected) extended along the *b* axis. Different rows are marked with arrows of different colors in Fig. 4, to illustrate this relatively complicated T-sheet. The tetrahedra in the interlayer single chain are described as T_i and marked with green arrows (with red profile). Each period contains two T_i chains

Table 1 Physical and optical properties of meifuite

Color	Colorless to pale green
Streak	White
Luster	Vitreous; transparent
Fluorescence	None
Hardness (Mohs)	3–4
Cleavage	{001} perfect
Parting	N/A
Tenacity	Sectile
Fracture	N/A
Optical Character	Biaxial (–)
Refractive Index	$\alpha = 1.628(1)$, $\beta \approx \gamma = 1.672(1)$
2V angle	~10°
Dispersion	N/A
Orientation	$n_\alpha \sim \perp$ (001)

https://doi.org/10.1007/s42860-021-00143-8 Published online by Cambridge University Press

Table 2 Results of the EPMA analysis of meifuite

	Elemental weight percentage (%)										Formula per 6 (Fe+Mg+Mn)									
	K	Na	Fe	Mg	Mn	Si	Al	O	Cl	H	Total	K	Na	Fe	Mg	Mn	Si	Al	O	Cl	OH
1	2.99	0.36	30.07	0.79	0.75	18.95	2.77	36.58	4.57	0.44	98.27	0.79	0.16	5.53	0.33	0.14	6.92	1.05	19.02	1.32	4.45
2	2.65	0.40	30.27	0.77	0.58	18.71	2.97	36.24	4.49	0.41	97.50	0.70	0.18	5.57	0.32	0.11	6.85	1.13	19.08	1.30	4.19
3	2.65	0.48	29.96	0.78	0.73	19.14	2.72	36.21	4.44	0.37	97.48	0.70	0.22	5.53	0.33	0.14	7.03	1.04	19.52	1.29	3.82
4	2.69	0.43	30.10	0.76	0.71	19.33	2.54	36.75	4.63	0.44	98.38	0.71	0.19	5.54	0.32	0.13	7.08	0.97	19.16	1.34	4.46
5	2.73	0.46	30.11	0.73	0.69	19.05	2.71	36.82	4.64	0.47	98.42	0.72	0.21	5.56	0.31	0.13	7.00	1.04	18.93	1.35	4.81
6	2.80	0.54	30.37	0.72	0.75	18.84	2.79	36.66	4.74	0.46	98.68	0.73	0.24	5.56	0.30	0.14	6.85	1.06	18.79	1.37	4.62
7	2.65	0.46	30.31	0.64	0.62	18.82	2.68	36.56	4.83	0.48	98.05	0.70	0.21	5.61	0.27	0.12	6.93	1.03	18.67	1.41	4.97
8	2.88	0.51	30.34	0.59	0.58	18.63	2.89	36.86	4.78	0.52	98.57	0.76	0.23	5.64	0.25	0.11	6.88	1.11	18.56	1.40	5.34
9	2.75	0.42	30.17	0.76	0.75	18.92	2.59	37.59	4.43	0.59	98.96	0.72	0.19	5.54	0.32	0.14	6.91	0.98	18.13	1.28	5.97
10	2.64	0.41	29.79	0.74	0.71	19.03	2.55	37.30	4.34	0.56	98.05	0.70	0.18	5.55	0.32	0.13	7.05	0.98	18.51	1.28	5.75
Ave.	2.74	0.45	30.15	0.73	0.69	18.94	2.72	36.76	4.59	0.47	98.24	0.72	0.20	5.56	0.31	0.13	6.95	1.04	18.84	1.33	4.84

that are related by inversion symmetry. Between the T_i chains, marked by the blue arrows in Fig. 4, are rows of T_h sites, which form a strip of hexagonal rings along the *b* axis. Each T_h site is part of at least one hexagonal ring (thus the name T_h), and T_{h1-4} are shared by two hexagonal rings. The remaining two rows of T sites, marked by red arrows in Fig. 4, are the T_s sites. The T_s chains are equivalent to the T_h strips cut in half. These incomplete hexagonal rings are connected to the T_i chains and form seven- and five-membered rings. Using terms describing the similar minnesotaite structure (Guggenheim & Eggleton, 1986b), meifuite has a 4+1+2+1 ($4T_h + 1T_i + 2T_s + 1T_i$) strip structure. Measuring the average T–O bond distances of the tetrahedra, the T_{h1-4} sites are larger than the other T sites, among which the T_{h1} and T_{h3} are the largest. These bond averages suggest that the Al is ordered into the T_{h1} and T_{h3} sites, obeying the Al-avoidance principle (Loewenstein, 1954). The hexagonal rings in the T sheets are significantly distorted from ideal shape due to this Al–Si ordering. The smaller edge T_h rows are twisted towards the T_i chains, and the other two corners can move to match the edge length of the larger middle T_h rows. Similar Al–Si ordering was reported in the structure of ganophyllite (Eggleton & Guggenheim, 1986), where Al prefers the central tetrahedral chain over the edge chains. This distortion distributes some of the stretching of the T sheets along the *a* axis into stretching along the *b* axis, making the T sheets a better match with the more symmetrical O sheets.

The A sites are cavities between the opposing T_h rings that are occupied partially by interlayer cations K and Na. No electron density was detected in the cavities associated with T_s and T_i sites. The A_1 sites are closer to the middle of the chain of hexagonal rings, which are 12 coordinated (14 if the A-Cl bonds are considered) in skewed hexagonal prism, similar to, but less symmetrical than, the interlayer site in the biotite structure. The A_2 sites, which are 12 coordinated in an irregular polyhedron, is less occupied than A_1 sites. Both A sites are relatively closely bonded to the tetrahedral oxygen near them, which suggest meifuite is unlikely to have a strong cation exchange capability as observed in ganophyllite (Guggenheim & Eggleton, 1986a), in which the interlayer cations are loosely bonded to only one T-sheet.

Because of the T-sheet modulation along the *a* axis, the O-sheet shows a wave-like shape along the *a* axis away from the T_h strips where the interlayer sites are occupied by K or Na, and towards the T_s strips where the interlayer sites are empty. The *c* axis is partially defined by the wave, because the T_h sites must directly oppose the T_s sites so that the expansion in one sheet is accommodated by the shrinking in the next. Some of the OH sites on the O-sheet (anion sites that are not shared with the T-sheet) are fully or partially substituted by Cl atoms. The Cl atoms, as shown in Fig. 4, are further away from the octahedral cations, resulting in longer Fe–Cl bonds than Fe–O bonds. It seems that only the OH site near the T_h and T_s rows can be replaced by Cl, and the Cl atom was not observed to replace the OH site associated with the T_i chains. The anion X_{2a} and X_{2b} sites are fully occupied by Cl with no evidence of OH.

Although the overall structure is triclinic, the O-sheet and T-sheet show monoclinic symmetry. The octahedra (ignoring the Cl substitution) preserve the mirror plane and 2-fold symmetry, although distorted along the body diagonal perpendicular to the *b* axis. In contrast, the distribution of the Cl atoms

https://doi.org/10.1007/s42860-021-00143-8 Published online by Cambridge University Press

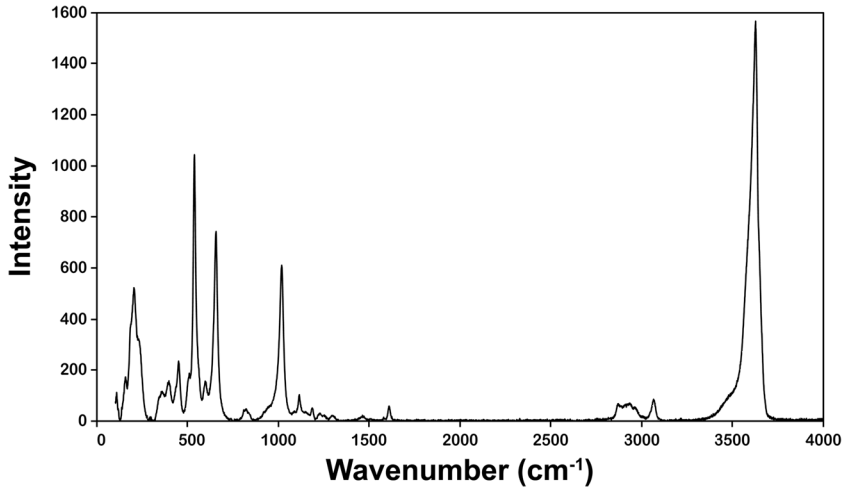

Fig. 3 Raman spectrum of meifuite. The strong peak at ~3630 cm^{-1} is from the structural OH group in the octahedral sheet

does not obey any higher symmetry than simple translation. The T-sheet shows *P*2/*b* symmetry with the 2-fold axis along the [100] direction. The glide planes and the 2-fold axes of the T-sheet are marked with red lines and arrows in Fig. 4. The *b* glide plane passes through the center of the T_h and T_s chains, and the 2-fold axes go through the T_{i2} and T_{i4} sites. This local symmetry produces non-space group extinction in the diffraction data. The 0*kl* reflections where $k = 2n+1$ are extinct as shown in the unwarped precession image in Fig. 5. As is found commonly in other crystals with layered structures, e.g. jinshajiangite, local pseudo-symmetry may often result in pseudo-merohedral twinning (Jin et al., 2018). In the case of meifuite, a 180° rotation around the [100] or [010] direction are possible twin laws for polysynthetic twinning along the [001] stacking direction. No obvious twin domains in the crystal studied have been detected, but these twin laws can almost certainly be found at a larger scale.

Stacking disorder is prominent in the meifuite structure, as often observed in layer silicate minerals and indicated by the streaking of reflections along [100]* directions. The streaking in the diffraction pattern (Fig. 5), however, is significantly weaker than that observed in the minnesotaite (Guggenheim & Eggleton, 1986b) or zussmanite structures (Jefferson, 1976), indicating larger domain sizes and fewer stacking errors. As shown in Fig. 5, the streaking in the diffraction pattern is found in both 0*kl* and *h*0*l* precession images, which indicates that the stacking faults that produce the disordered stacking occur both along the [100] and [010] directions. Moreover, weak intensities can be observed between (00*l*) reflections (marked with blue arrow in Fig. 5), which suggest the presence of chemical disorder between layers, instead of pure structural stacking disorder.

An apparent number of tetrahedral site vacancies were observed in the structure refinement, which were explained by the stacking disorder in the structure. Stacking faults in the real structure randomly misalign the tetrahedral sites from one layer to the next, which are reflected as "missing" T-site atoms in the refined structure. These "missing" T-site atoms contribute to the electron density peaks in the empty spaces between the T sites (i.e. the center of the hexagonal rings between the T_h sites). A structure with partially occupied Si and Al sites assigned to the positions between T-sites has been refined to better account for the stacking disorder in the structure, which resulted in a composition much closer to the EPMA analysis. The crystallographic information file (CIF) of the structure model with extra T sites can be found in the Supplementary Material (meifuite-minnesotaite.cif). The refined occupancies of the interlayer cation sites A_1 and A_2 might have been affected in a similar way. The stacking disorder affects minimally the O-sheet, because the octahedral sites repeat every 1/8*a* and 1/3*b*; thus the sites are always aligned despite the stacking faults. This is why the (0*k*0) and (*h*00) reflections with $k = 3n$ or $h = 8n$, of which the intensities are contributed mainly by the heavy Fe atoms, were always sharp and strong with no obvious streaking. Some irregular shape in the electron densities around Fe atoms was observed in the structure refinement, reflecting the misaligned waviness of the O-sheet resulting from the stacking disorder.

The ratio between the number of tetrahedral and octahedral sites did not change relative to talc or mica. The T_i tetrahedra disconnect a single row of tetrahedra from the octahedral sheet and connect them to the next 2:1 layer. These T_i sites, which bridge two adjacent T–O–O–T sheets, share all four corners with other tetrahedra, whereas the T_h and T_s sites, which are connected to the O-sheet, share only three corners with other tetrahedra. This arrangement changes the number of bridging oxygen atoms relative to the talc or mica structure.

The Na substitution and vacancies in the interlayer A sites should be the main cause of chemical variations in meifuite. The Al/Si ratio in the T-sheet should be relatively constant to balance the charge of interlayer cations. How much Mg can be accommodated in the O-sheet of the meifuite structure before it becomes unstable is unclear. Up to ~35% Mg has been reported in the O-sheet of minnesotaite; a change in the T-sheet structure is expected when the Mg/Fe ratio exceeds 0.2, however (Guggenheim & Eggleton, 1986b). The Cl/OH ratio is not expected to vary much in meifuite, because only a small fraction of the OH sites can be substituted by Cl in the

https://doi.org/10.1007/s42860-021-00143-8 Published online by Cambridge University Press

Table 3 Experimental and crystallographic information of meifuite

		Meifuite
Crystal data		
Chemical formula from structure		$K_{0.594}Na_{0.206}Fe_{5.856}Mg_{0.144}Al_{0.954}Si_{6.411}O_{19}(OH)_{4.432}Cl_{1.568}$
a, *b*, *c* (Å)		22.7773(13)
		9.5553(5)
		14.3282(8)
α, β, γ (°)		99.258(4)
		136.750(3)
		89.899(4)
V (Å^3)		2077.9(2)
Z		2
Crystal size (mm)		0.05×0.04×0.03
Data collection		
Exposure time (s/frame)		65
Scanning width (°)		0.5
Runs		4ω+1φ
Total reflections		46699
Independent reflections		12728
Observed [I > 3σ(I)] reflections		3757
R_{int}		0.235*
θ values (°)		1.32
		30.73
(sin θ/λ)max (Å^{-1})		0.715
Range of *h*, *k*, *l*	*h*	-32→32
	k	-13→13
	l	-20→20
Refinement		
R[F^2>3σ(F^2)]		0.0749
R(all)		0.1837
GOF (all)		1.41
GOF (obs)		2.52
No. of parameters		504
No. of constraints		46
$\Delta\rho_{max}$, $\Delta\rho_{min}$ (eÅ^{-3})		5.59, -3.42

*The R_{int} value is from unmerged integrated intensities without absorption correction. Absorption corrected. *hkl* file has an R_{int} of 0.06, but the R values in the structure refinement increase and, therefore, were not used.

structure. Therefore, the general chemical formula of meifuite is (K,Na,□) (Fe,Mg,Mn)$_6$(Si,Al)$_8$O$_{19}$(OH,Cl)$_6$, with an ideal formula of $KFe_6(AlSi_7)O_{19}(OH)_4Cl_2$.

DISCUSSION

Several ferrous phyllosilicate minerals, including annite, stilpnomelane, minnesotaite, greenalite, and zussmanite (e.g. Table 6 for 2:1 layer examples) are found commonly in Fe-rich rocks. Each has a similar chemical composition to meifuite, and the crystal structures are also strongly related to each other.

The structure that is most closely related to meifuite is certainly minnesotaite. Although a crystal structure refinement of minnesotaite is unavailable, structure models were constructed from high-resolution transmission electron microscope (HRTEM) images and selected area electron diffraction (SAED) pattern (Guggenheim & Eggleton, 1986b). This approach is the case for many modulated layer silicate structures such as greenalite (Guggenheim & Eggleton, 1998), where small crystal size and stacking disorder make a structure refinement impossible. The structure of minnesotaite also has a continuous

https://doi.org/10.1007/s42860-021-00143-8 Published online by Cambridge University Press

Table 4 Atomic coordinates of the meifuite structure

Site	Atom	Occupancy	*x*	*y*	*z*	U_{eq}
A_1	K Na	0.696(17) 0.154(17)	0.4471(2)	0.2485(4)	0.5034(4)	0.042(3)
A_2	K Na	0.538(17) 0.162(17)	0.6605(2)	0.2468(4)	0.5014(4)	0.022(3)
T_{h1}	Al	0.983(7)	0.54562(17)	0.6020(3)	0.7335(3)	0.006072
T_{h2}	Si	0.946(6)	0.66174(17)	0.4278(3)	0.7334(3)	0.006899
T_{h3}	Al	0.971(7)	0.66799(17)	0.1007(3)	0.7332(3)	0.004895
T_{h4}	Si	0.948(6)	0.55281(17)	0.9298(3)	0.7358(3)	0.006899
T_{h5}	Si	0.964(6)	0.77353(16)	0.9215(3)	0.7163(3)	0.006253
T_{h6}	Si	0.947(6)	0.76698(17)	0.6006(3)	0.7172(3)	0.006604
T_{h7}	Si	0.960(6)	0.42436(17)	0.4243(3)	0.7166(3)	0.006604
T_{h8}	Si	0.936(6)	0.56782(17)	0.8986(3)	0.2798(3)	0.006253
T_{s1}	Si	0.921(6)	0.96412(17)	0.7326(3)	0.2932(3)	0.005653
T_{s2}	Si	0.933(6)	0.85644(17)	0.5571(3)	0.3025(3)	0.005653
T_{s3}	Si	0.931(6)	0.85031(17)	0.2340(3)	0.2991(3)	0.005859
T_{s4}	Si	0.947(6)	0.96244(16)	0.0552(3)	0.2978(3)	0.006533
T_{i1}	Si	0.882(6)	0.76452(17)	0.9756(3)	0.4957(3)	0.005653
T_{i2}	Si	0.894(6)	0.14502(17)	0.2505(3)	0.4989(3)	0.005653
T_{i3}	Si	0.887(6)	0.76974(17)	0.5229(3)	0.5062(3)	0.005653
T_{i4}	Si	0.902(6)	0.15722(17)	0.7492(3)	0.4973(3)	0.005653
M_1	Fe	1	0	0	0	0.007928
M_2	Fe	1	½	0	0	0.006741
M_3	Fe	1	0.99332(9)	0.66470(15)	0.99339(15)	0.007928
M_4	Fe	1	0.50174(9)	0.33700(15)	0.99979(15)	0.007002
M_5	Fe Mg	0.941(6) 0.059(6)	0.75917(9)	0.00156(14)	0.01904(14)	0.006611
M_6	Fe Mg	0.966(6) 0.034(6)	0.75713(8)	0.66367(14)	0.01869(14)	0.006024
M_7	Fe Mg	0.970(6) 0.030(6)	0.76002(9)	0.33134(14)	0.01925(15)	0.007053
M_8	Fe Mg	0.986(6) 0.014(6)	0.63364(8)	0.16569(14)	0.01805(14)	0.007638
M_9	Fe Mg	0.913(6) 0.087(6)	0.87931(9)	0.83255(15)	0.01101(15)	0.006596
M_{10}	Fe Mg	0.997(6) 0.004(6)	0.63341(8)	0.50486(14)	0.01956(14)	0.007557
M_{11}	Fe	1	0.88059(8)	0.15980(14)	0.01159(13)	0.006133
M_{12}	Fe	1	0.63379(9)	0.83273(14)	0.01649(14)	0.006974
M_{13}	Fe	1	0.87632(8)	0.49969(14)	0.00709(13)	0.005814
O_1	O	1	0.7459(4)	0.4714(6)	0.9070(6)	0.007853
O_2	O	1	0.6251(4)	0.6408(6)	0.9090(6)	0.005842
O_3	O	1	0.6286(4)	0.9727(6)	0.9081(6)	0.007853
O_4	O	1	0.7498(4)	0.1401(6)	0.9075(6)	0.004966
O_5	O	1	0.8583(4)	0.9649(6)	0.8802(6)	0.007853
O_6	O	1	0.8544(4)	0.6353(6)	0.8794(6)	0.007853
O_7	O	1	0.4882(4)	0.4700(6)	0.8790(6)	0.007853
O_8	O	1	0.5100(4)	0.8652(6)	0.1210(6)	0.007853
O_9	O	1	0.8905(4)	0.6927(6)	0.1255(6)	0.006836
O_{10}	O	1	0.7707(4)	0.5225(6)	0.1351(6)	0.007853
O_{11}	O	1	0.7685(4)	0.1933(6)	0.1319(6)	0.006735

https://doi.org/10.1007/s42860-021-00143-8 Published online by Cambridge University Press

Table 4 (continued)

Site	Atom	Occupancy	*x*	*y*	*z*	U_{eq}
O_{12}	O	1	0.8933(4)	0.0230(6)	0.1308(6)	0.008914
O_{13}	O	1	0.5765(4)	0.4925(8)	0.6757(7)	0.023778
O_{14}	O	1	0.5244(4)	0.7550(7)	0.6745(7)	0.018175
O_{15}	O	1	0.5858(4)	0.9913(8)	0.6771(7)	0.021618
O_{16}	O	1	0.6966(4)	0.0096(8)	0.6636(7)	0.024164
O_{17}	O	1	0.7330(4)	0.7501(7)	0.6674(6)	0.017791
O_{18}	O	1	0.6881(4)	0.4994(7)	0.6697(6)	0.017163
O_{19}	O	1	0.4526(4)	0.5092(7)	0.6623(7)	0.01782
O_{20}	O	1	0.5792(4)	0.7494(7)	0.3282(7)	0.024452
O_{21}	O	1	0.4704(4)	0.0048(7)	0.6758(7)	0.018767
O_{22}	O	1	0.6355(4)	0.2514(7)	0.6740(7)	0.017511
O_{23}	O	1	0.9354(4)	0.6498(7)	0.3472(6)	0.018775
O_{24}	O	1	0.8843(4)	0.4076(7)	0.3540(6)	0.014605
O_{25}	O	1	0.9267(4)	0.1495(8)	0.3484(6)	0.018093
O_{26}	O	1	0.9831(4)	0.9063(7)	0.3501(6)	0.015045
O_{27}	O	1	0.2196(4)	0.1522(7)	0.5718(7)	0.017835
O_{28}	O	1	0.1539(4)	0.3514(7)	0.4284(7)	0.018295
O_{29}	O	1	0.7824(4)	0.3713(7)	0.4606(7)	0.02501
O_{30}	O	1	0.8200(4)	0.1288(7)	0.5433(7)	0.02088
O_{31}	O	1	0.7949(4)	0.9412(7)	0.6313(7)	0.021508
O_{32}	O	1	0.7802(4)	0.5126(7)	0.6276(7)	0.020397
O_{33}	O	1	0.6756(4)	0.5557(8)	0.3705(7)	0.022755
O_{34}	O	1	0.6610(4)	0.9871(7)	0.3694(7)	0.021974
O_{35}	O	1	0.0540(4)	0.6780(7)	0.3588(7)	0.016609
O_{36}	O	1	0.8393(4)	0.6495(7)	0.3824(7)	0.019705
O_{37}	O	1	0.8228(4)	0.1846(7)	0.3685(6)	0.01688
O_{38}	O	1	0.0513(4)	0.1482(7)	0.3734(7)	0.020529
X_1a	Cl	0.327(9)	0.6061(5)	0.2965(8)	0.8608(9)	0.008765
	OH	0.673(9)	0.6303(8)	0.3093(11)	0.9167(14)	0.008765
X_1b	Cl	0.184(9)	0.7217(9)	0.7924(14)	0.8543(16)	0.008765
	OH	0.816(9)	0.7502(6)	0.8060(9)	0.9130(12)	0.008765
X_2a	Cl	1	0.46380(17)	0.7910(3)	0.8309(3)	0.021158
X_2b	Cl	1	0.84163(15)	0.2898(2)	0.8350(3)	0.014922
X_{s1}	OH	0.666(9)	0.7669(7)	0.8585(11)	0.1245(14)	0.008765
	Cl	0.334(9)	0.7877(5)	0.8697(8)	0.1834(8)	0.008765
X_{s2}	OH	0.746(8)	0.8893(7)	0.3563(9)	0.1171(12)	0.008765
	Cl	0.254(8)	0.9206(6)	0.3695(10)	0.1777(11)	0.008765
OH_1	OH	1	0.6277(4)	0.0179(6)	0.1055(6)	0.008274
OH_2	OH	1	0.6319(4)	0.3580(6)	0.1102(6)	0.008274
OH_3	OH	1	0.6262(4)	0.6930(6)	0.1080(6)	0.008274
OH_4	OH	1	0.0042(4)	0.8563(6)	0.1037(6)	0.008274
OH_5	OH	1	0.9991(4)	0.4798(6)	0.9014(6)	0.006063
OH_6	OH	1	0.0062(4)	0.1907(6)	0.1048(6)	0.008274

trioctahedral sheet (O-sheet) filled with Fe(II) sandwiched by two tetrahedral sheets (T-sheet), which are modulated by interlayer tetrahedral chains along the *a* axis every other four or five tetrahedral rows. Minnesotaite differs from meifuite mainly by the absence of interlayer cations (K or Na) and no (or very little) Al substitution in the T

https://doi.org/10.1007/s42860-021-00143-8 Published online by Cambridge University Press

Table 5 Interatomic distances (Å) in the meifuite structure

A_1 3.173	O_{15}	2.788(10)	T_{s1} 1.621	O_9	1.603(7)	M_6 2.134 2.211	X_{s1OH}	2.101(15)
	O_{13}	2.790(7)		O_{23}	1.609(12)		X_{1bOH}	2.113(8)
	O_{17}	2.864(8)		O_{26}	1.631(7)		O_1	2.117(16)
	O_{20}	2.876(14)		O_{35}	1.642(9)		O_2	2.137(8)
	O_{22}	3.014(9)	T_{s2} 1.611	O_{23}	1.603(12)		O_{10}	2.160(9)
	O_{19}	3.028(10)		O_{10}	1.604(10)		O_9	2.179(8)
	O_{16}	3.041(8)		O_{36}	1.612(6)		X_{1bCl}	2.42(2)
	O_{14}	3.049(14)		O_{24}	1.625(7)		X_{s1Cl}	2.459(10)
	O_{21}	3.427(11)	T_{s3} 1.617	O_{25}	1.601(6)	M_7 2.128 2.209	O_1	2.102(9)
	X_{1bCl}	3.433(10)		O_{11}	1.603(9)		O_4	2.116(8)
	X_{1aCl}	3.443(15)		O_{37}	1.632(13)		X_{s2OH}	2.125(17)
	O_{18}	3.493(8)		O_{24}	1.634(7)		X_{1aOH}	2.139(16)
	O_{15}	3.564(8)	T_{s4} 1.614	O_{38}	1.600(9)		O_{10}	2.141(8)
	O_{13}	3.609(12)		O_{12}	1.605(7)		O_{11}	2.148(9)
A_2 3.098	O_{18}	2.822(9)		O_{26}	1.623(8)		X_{1aCl}	2.392(9)
	O_{21}	2.855(7)		O_{25}	1.627(11)		X_{s2Cl}	2.512(12)
	O_{34}	2.873(10)	T_{i1} 1.630	O_{31}	1.615(11)	M_8 2.152 2.191	OH_1	2.097(9)
	O_{22}	2.908(14)		O_{30}	1.623(8)		OH_2	2.102(8)
	O_{32}	2.919(8)		O_{27}	1.639(10)		X_{1aOH}	2.116(19)
	O_{14}	2.934(9)		O_{34}	1.642(7)		O_3	2.167(8)
	O_{16}	3.181(10)	T_{i2} 1.605	O_{36}	1.589(11)		O_{11}	2.174(8)
	O_{19}	3.242(8)		O_{27}	1.607(7)		O_8	2.253(7)
	X_2a	3.260(6)		O_{38}	1.612(6)		X_{1aCl}	2.425(13)
	X_2b	3.269(4)		O_{28}	1.613(11)	M_9 2.144 2.189	OH_4	2.076(9)
	O_{30}	3.443(12)	T_{i3} 1.607	O_{32}	1.595(12)		O_{12}	2.135(15)
	O_{29}	3.475(14)		O_{29}	1.606(9)		X_{1bOH}	2.136(8)
T_{h1} 1.690	O_2	1.676(7)		O_{33}	1.611(6)		O_9	2.152(9)
	O_{13}	1.685(12)		O_{28}	1.619(9)		O_6	2.175(7)
	O_{19}	1.697(10)	T_{i4} 1.625	O_{29}	1.609(8)		O_5	2.190(9)
	O_{14}	1.698(8)		O_{30}	1.621(11)		X_{1bCl}	2.462(17)
T_{h2} 1.643	O_{13}	1.631(10)		O_{37}	1.624(11)	M_{10} 2.157 2.199	OH_2	2.076(9)
	O_{18}	1.631(12)		O_{35}	1.644(6)		OH_3	2.106(8)
	O_{22}	1.651(7)	M_1 2.173	OH_6	2.099(7)		O_2	2.111(9)
	O_1	1.661(6)		OH_4	2.133(9)		X_{1aOH}	2.151(16)
T_{h3} 1.675	O_{15}	1.666(6)		O_5	2.286(8)		O_{10}	2.218(8)
	O_4	1.670(10)	M_2 2.138 2.247	OH_1	2.072(8)		O_7	2.278(7)
	O_{16}	1.678(8)		O_8	2.204(9)		X_{1aCl}	2.452(10)
	O_{22}	1.685(12)		X_2a	2.465(3)	M_{11} 2.140 2.237	OH_6	2.090(8)
T_{h4} 1.636	O_{21}	1.618(9)	M_3 2.140 2.210	OH_5	2.092(8)		X_{s2OH}	2.122(13)
	O_{15}	1.638(7)		OH_4	2.101(8)		O_4	2.138(8)
	O_{14}	1.643(13)		OH_5	2.121(9)		O_{12}	2.169(9)
	O_3	1.646(7)		OH_6	2.130(9)		O_5	2.181(7)
T_{h5} 1.623	O_5	1.580(5)		O_6	2.256(8)		X_{s2Cl}	2.412(12)
	O_{16}	1.619(9)		X_2b	2.562(3)		X_2b	2.543(4)
	O_{31}	1.642(13)	M_4 2.154 2.209	OH_3	2.065(8)	M_{12} 2.119 2.228	OH_1	2.075(8)
	O_{17}	1.649(7)		OH_2	2.097(8)		O_2	2.103(8)
T_{h6} 1.617	O_6	1.577(5)		O_7	2.153(9)		OH_3	2.104(9)
	O_{18}	1.625(10)		O_7	2.205(8)		O_3	2.149(9)
	O_{17}	1.631(12)		O_8	2.247(8)		X_{s1OH}	2.166(16)

https://doi.org/10.1007/s42860-021-00143-8 Published online by Cambridge University Press

Table 5 (continued)

	O_{32}	1.634(7)		X_2a	2.486(5)		X_{s1Cl}	2.377(8)
T_{h7} 1.623	O_7	1.570(7)	M_5 2.128 2.211	X_{s1OH}	2.103(8)	M_{13} 2.130 2.228	X_2a	2.624(3)
	O_{19}	1.617(12)		O_3	2.111(19)		OH_5	2.076(8)
	O_{33}	1.648(9)		X_{1bOH}	2.116(12)		X_{s2OH}	2.113(16)
	O_{20}	1.659(8)		O_4	2.129(9)		O_9	2.139(8)
T_{h8} 1.599	O_8	1.554(8)		O_{11}	2.137(8)		O_1	2.151(8)
	O_{34}	1.598(8)		O_{12}	2.170(8)		O_6	2.169(9)
	O_{21}	1.622(12)		X_{1bCl}	2.419(18)		X_{s2Cl}	2.433(15)
	O_{20}	1.624(9)		X_{s1Cl}	2.506(12)		X_2b	2.510(4)

sheet. The relationship between meifuite and minnesotaite is analogous to phlogopite and talc.

A structure model of minnesotaite (*P*-cell) was constructed based on the meifuite structure, which is illustrated in Fig. 6. The structure of the minnesotaite from first-principles calculation is provided in the Supplementary Material (meifuite-minnesotaite.cif). The structure shown in Fig. 6 was modified slightly to display a wave-like octahedral sheet similar to that in the meifuite structure, to represent the structure model and TEM observation made by Guggenheim and Eggleton (1986b). Simulated electron diffraction patterns of the minnesotaite structure model can also be found in Fig. S1, which are very similar to the diffraction pattern reported by Guggenheim and Eggleton (1986b).

The hexagonal rings of tetrahedra from adjacent T-sheets are not always "superimposed" or matched as suggested by Guggenheim and Eggleton (1986b). Some hexagonal rings (blue arrows in Fig. 6) from opposing T sheets match with each other, creating the same 12-coordinated cavities that can be occupied by K atoms in the meifuite structure (sites between the T_h tetrahedra). Other hexagonal rings from opposing T sheets (red arrows in Fig. 6) are offset, leaving no regular cavities that can accommodate interlayer cations. These hexagonal rings have a similar configuration as the T_s rows in the meifuite structure, only wider. This is the only possible topology for the minnesotaite (*P*-cell) structure, with alternating rows of hexagonal rings that match and offset, so that the interlayer tetrahedral chain can connect the 2:1 layers. Thus, two polytypes can occur for the *C*-cell minnesotaite structure by deleting one tetrahedral row on the T-sheet edge from either the matched rings (blue arrow) or the offset rings (red arrow). With no interlayer cations filling the gap, neither of the two polytypes is obviously favorable over the other, and disorder between the two may be common. The T sheets of the *C*-cell minnesotaite structure has a local symmetry of *C*2/*m*, with mirror planes going through the centers of the three-rowed strips, instead of a glide plane.

Strip units of different widths and sequences were reported in the minnesotaite structure (Ahn & Buseck, 1989). The hexagonal rings in the T sheets of minnesotaite are nearly ideal hexagons without Al substituting Si in the tetrahedra, which suggests that the strips in the minnesotaite structure are more compatible with the T_i chains. As shown in Fig. 6, the width of each tetrahedral strip (number of rows) does not change the position of the bridging oxygen on the edge, leaving it always available to connect to the T_i chains. Therefore, 5-row or 3-row strips may occur in the structure. The meifuite structure, on the other hand, is not as flexible, due to the Al–Si ordering and distortion of the hexagonal rings.

In the structure model (Fig. 6) proposed by Guggenheim and Eggleton (1986b), the stacking direction along the *c* axis aligns the T_i chains of one layer with the center of T_h rows of the next layer. Thus, the wave-like characteristic of the O-sheet matches the T-sheets above and beneath, and the wave always bends towards the T_i chain and away from the T_h rows. In the structure of mica or talc, where no tetrahedra connect the two adjacent T-sheets, the O-sheets would be perfectly flat, constrained by equal tension on both sides. The waviness of the O-sheet in minnesotaite is determined by the interlayer T_i chains, which constrain the distances between two adjacent layers at the connected points. A minnesotaite sample with a β* angle of 64° instead of 52° was reported by Ahn and Buseck (1989), however (Fig. 6). The hypothetical structure with displacement of tetrahedral strips by (2/10)*a* from the 52° structure, showing the "most 2:1 layer characteristics" (i.e. the T_h strips match each other on opposite sides of the O sheet), was never observed. This seems to suggest that the different stacking sequences have little effect on the energy of the structure, as long as the T_i chains are not aligned directly across the O-sheet, which would presumably destabilize the octahedral sites in between.

Layer stacking in meifuite shows the alignment of the center of T_s strips with the center of T_h strips on the opposite side of the O-sheet, resulting in a slightly more complicated wave in the O-sheet. Unlike the minnesotaite structure, the interlayer cations (K, Na) introduce constraints on the shape of the O-sheet, in addition to the interlayer T_i chains. By matching the center of T_h strips with T_s strips, the structure forms the large cavities between the T-sheets to accommodate interlayer cations. Although the streaking in the diffraction pattern of meifuite is strong due to stacking faults, polytypes with different stacking patterns, as observed in the minnesotaite structure, should not be possible for meifuite.

The Raman spectra of the phyllosilicate minerals were summarized and discussed by Wang et al. (2015) who suggested that Raman is effective for phase identification. The Raman spectrum of meifuite (Fig. 3) is unique amongst phyllosilicates. Most silicate minerals show the skeleton vibrations below 1100 cm^{-1} and (OH) or H_2O stretching mode above 3400 cm^{-1}, with essentially no signals between them. The Raman

https://doi.org/10.1007/s42860-021-00143-8 Published online by Cambridge University Press

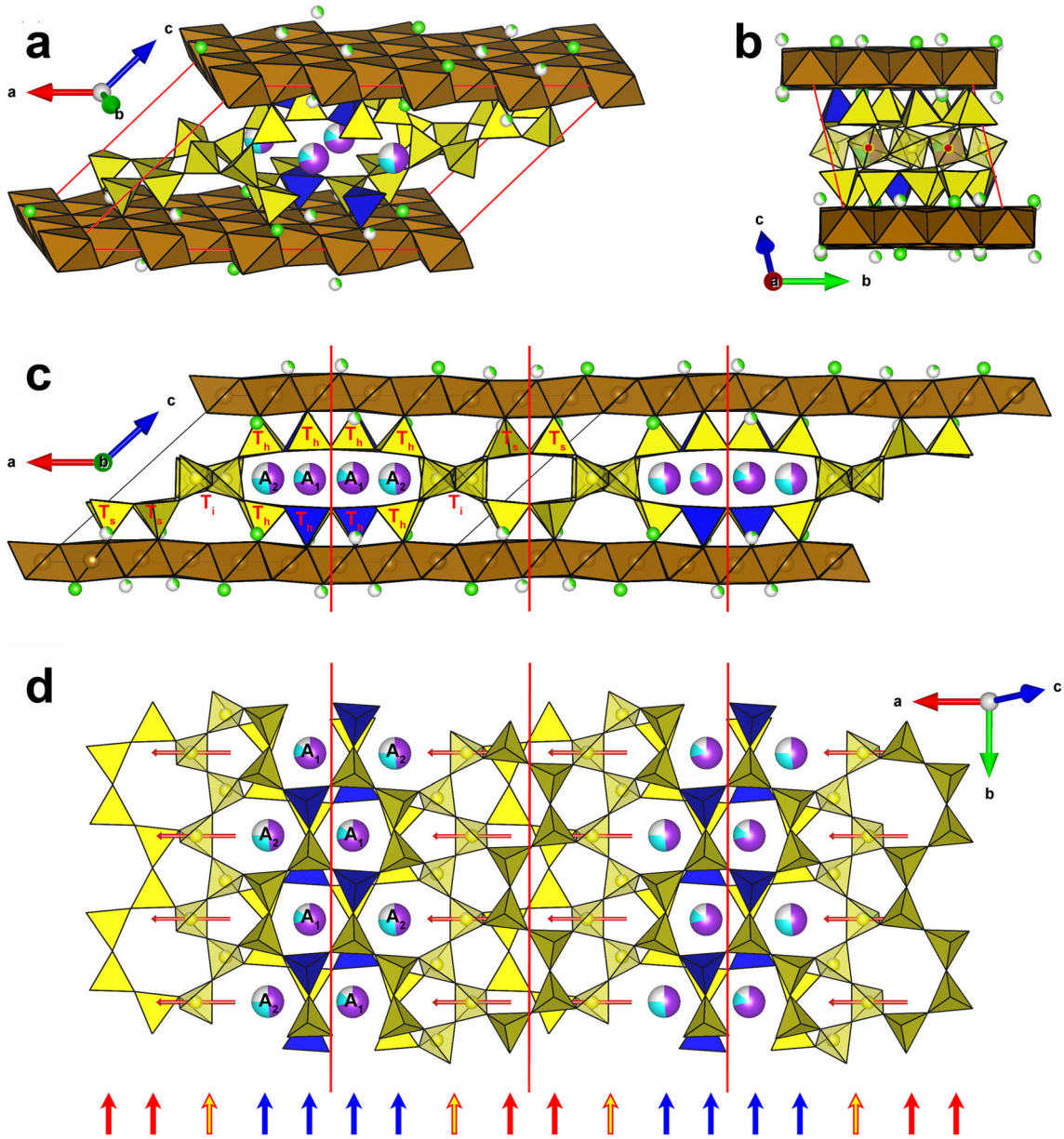

Fig. 4 The crystal structure of meifuite projected along different directions. Only the largest T_{h1} and T_{h3} sites are refined as Al in the structure and shown as blue tetrahedra, and all the other tetrahedra are colored yellow as Si sites. The K and Na atoms are colored purple and cyan, respectively. The Cl atoms are shown as green balls next to the octahedral sheet. The strip structure of the T sheets are best seen projected along the *b* axis in part **c**. The interlayer cations are found between the wider strips. The opposing T sheets along with the interlayer cations display a *P*2/*b* local symmetry, with the local *b*-glide planes and 2-fold symmetry marked with red lines and arrows through the silicon atoms

spectrum of meifuite shows peaks below ~1600 cm^{-1} for the skeleton vibrations, and small peaks at ~3000 cm^{-1}. The strong Raman shift between 600 and 800 cm^{-1} is the Si–O_b–Si peak in silicate structures, which is observed in nearly all chain and layer silicate structures (figs 6–15 in Wang et al., 2015). The Si–O_b–Si peak of the meifuite structure (Fig. 3) appears near 655 cm^{-1}, which is a much lower wavenumber than the 700 cm^{-1} common to most phyllosilicate minerals. The chain silicates, in contrast, commonly show the Si–O_b–Si peak at a lower wavenumber. For instance, grunerite, the Fe endmember of amphiboles with double chain strips, shows a strong Si–O_b–Si peak at ~660 cm^{-1} (Leissner, 2014), and this is consistent with the peak in the strip structures and interlayer chains of meifuite. The Si–O_b–Si peak in the Raman spectrum of minnesotaite (Wang et al., 2015), which was misinterpreted as Fe-rich talc in their paper, is also shifted toward the lower wavenumber relative to talc. The strong Raman shift at 536 cm^{-1} seems to be characteristic of Fe-rich phyllosilicate minerals as suggested by Wang et al. (2015).

The strong Raman shift at 3630 cm^{-1} from the stretching of the OH group of meifuite in the octahedral sheets appears

https://doi.org/10.1007/s42860-021-00143-8 Published online by Cambridge University Press

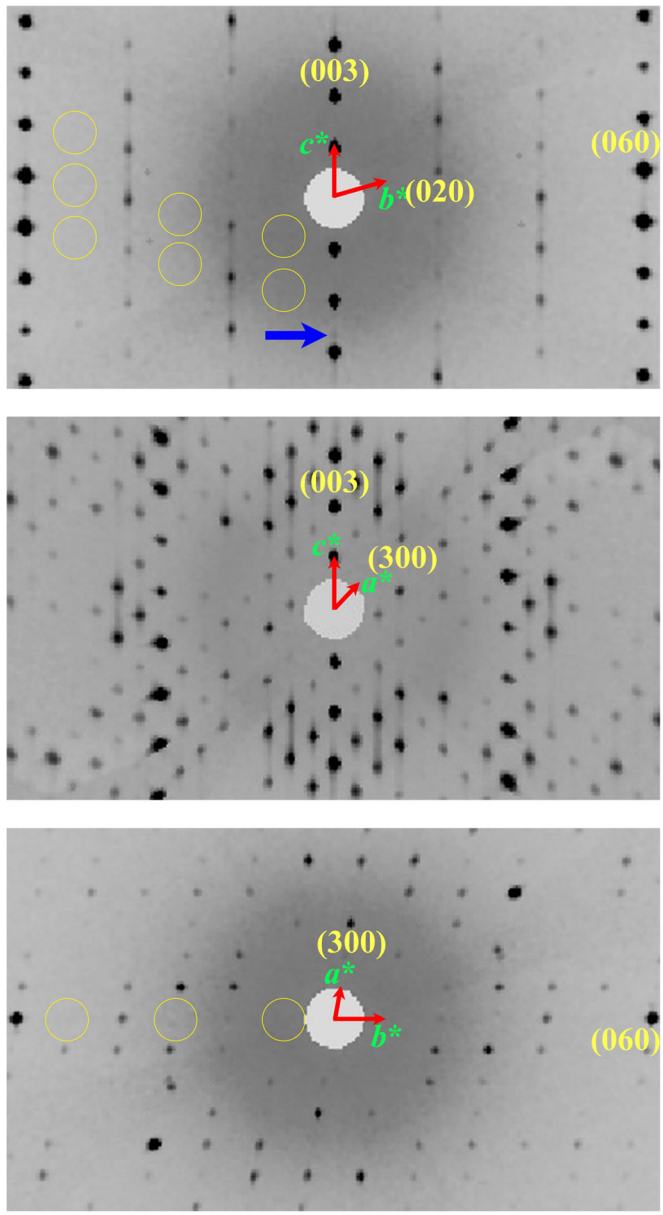

Fig. 5 Unwarped precession images from the XRD data of meifuite. From top to bottom: (0*kl*), (*h*0*l*), (*hk*0). The (0*kl*) reflections where k = odd are completely absent in the diffraction pattern (marked by yellow circles), indicating the pseudo-glide plane symmetry of the T sheets is nearly perfect. The blue arrow marks the streaking between (00*l*) reflections

much broader than those of talc and mica. However, the peak is well defined with a small shoulder toward the lower wavenumber side, and no broad hump is observed as in montmorillonite, where water molecules are present in the structure. The broadness of the OH stretching peak in the Raman spectrum is probably determined by the symmetry of the structure. In the structures of mica-1M or talc-1A, all the OH groups are symmetrically equivalent, therefore their stretching mode is the same. In structures such as kaolinite, the OH groups on either side of the octahedral sheets are symmetrically independent, and produce uniquely different OH-stretching peaks in the Raman spectra. Meifuite has a symmetry of $P\bar{1}$, with 10 symmetrically independent OH groups in the structures, some partially substituted by Cl. These OH groups have similar local environments, but the differences are also obvious. Similar broadening of the OH-stretching peak is also observed in minnesotaite (Wang et al., 2015), which has a triclinic symmetry with many symmetrically independent OH groups.

The composition of meifuite falls between annite and minnesotaite (see 3Fe normalized formula in Table 6). Meifuite is also close to stilpnomelane in Al/Si content.

https://doi.org/10.1007/s42860-021-00143-8 Published online by Cambridge University Press

Table 6 Comparisions among known ferrous phyllosilicates with 2:1 structure

Mineral	Annite	Meifuite	Stilpnomelane	Zussmanite	Minnesotaite
Ideal Chemical Formula	$KFe_3AlSi_3O_{10}(OH, F)_2$	$KFe_6AlSi_7O_{19}(OH, Cl)_6$	$K_5Fe_{48}Al_9Si_{63}O_{165}(OH)_{48}.12H_2O$	$KFe_{13}AlSi_{17}O_{42}(OH)_{14}$	$Fe_{30}Si_{40}O_{96}(OH)_{28}$
Normalized to 3Fe	$KFe_3AlSi_3O_{10}(OH,F)_2$	$K_{0.5}Fe_3Al_{0.5}Si_{3.5}O_{9.5}(OH, Cl)_3$	$K_{0.3125}Fe_3Al_{0.5625}Si_{3.9375}O_{10.3125}(OH)_3.0.75H_2O$	$K_{0.23}Fe_3Al_{0.23}Si_{3.92}O_{9.69}(OH)_{3.23}$	$Fe_3Si_4O_{9.6}(OH)_{2.8}$
Crystal System	monoclinic	triclinic	triclinic	trigonal	triclinic
Space Group	$C2/m$	$P\bar{1}$	$P\bar{1}$	$R\bar{3}$	$P\bar{1}$
Color	dark brown	pale green	dark green	pale green	pale green
Birefringence	0.066	0.044	0.33	0.020	0.037-0.040
X-ray diffraction pattern character	Strongest peak: (001) ~10.3 Å	(001) ~9.5 Å, (002) stronger than (003), strong peak at ~2.69 Å	(001) peak at ~12.2 Å	(003) ~9.5 Å, (006) peak stronger than (009) peak.	(001) ~9.5 Å, (002) peak weaker than (003) peak

(Eggleton & Bailey, 1964; Lopes-Vieira & Zussman, 1969; Eggleton, 1972; Eggleton & Chappell, 1978; Guggenheim & Bailey, 1982)

Therefore, comparing the stability of meifuite to stilpnomelane is useful, though limited by the single known occurrence of meifuite. A detailed thermodynamic analysis is also beyond the scope of the present paper. The chemical systems containing ferrous phyllosilicate minerals are very complicated, with several components involved, and both temperature and

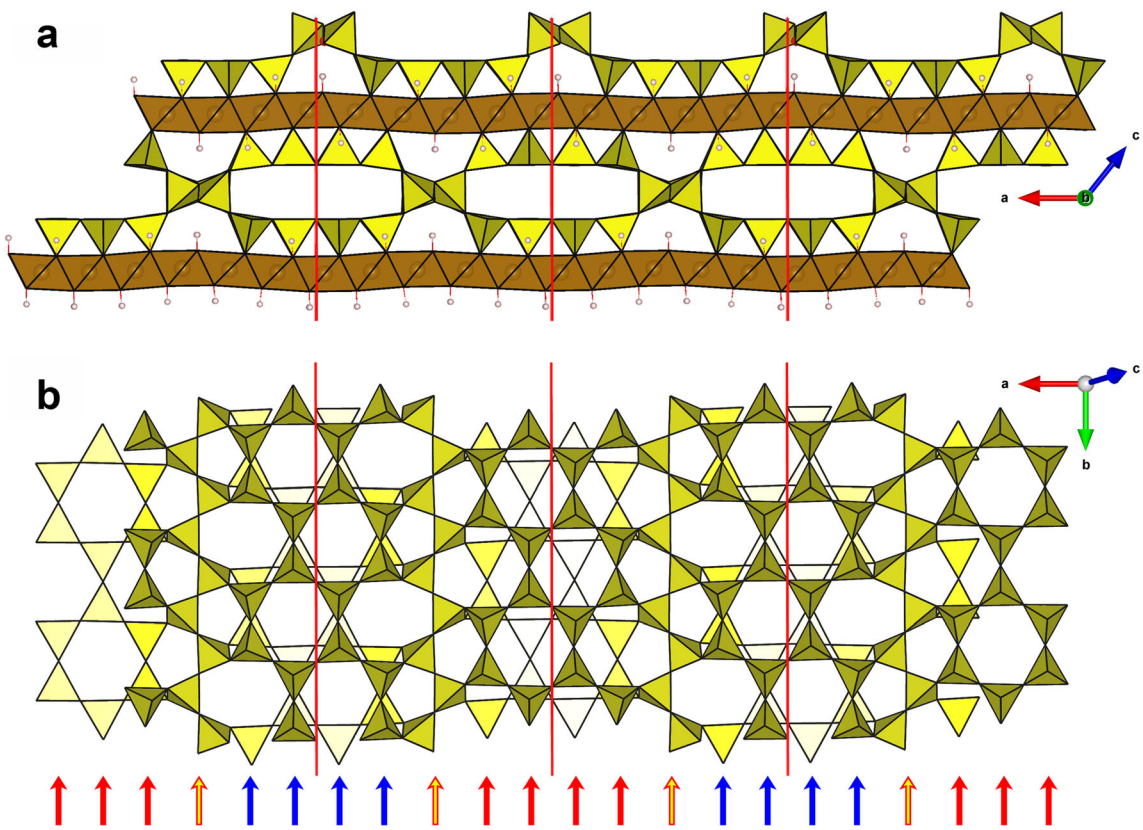

Fig. 6 The idealized crystal structure of minnesotaite projected along **a** the *b* axis and **b** the *c** axis. The blue and red arrows in the figure mark two different types of T-strips in the structure. The hexagonal rings in the blue strips are matched with each other, whereas in the red strips the hexagonal rings are offset from each other. The yellow arrows with red outline mark the interlayer tetrahedral chain. The red lines mark the local glide planes in the T sheets

https://doi.org/10.1007/s42860-021-00143-8 Published online by Cambridge University Press

pressure playing important roles. Fe-rich, low-grade metamorphic systems have been studied extensively, in attempts to place constraints on the conditions of formation of different ferrous phyllosilicate minerals (Blake, 1965; Brown, 1971; Klein, 1974; Miyano, 1982). Nothing similar to meifuite, however, has been reported in these systems, indicating something quite unique about the Yinachang Fe-Cu-REE deposit.

The phase equilibria in the system K_2O-FeO-MgO-Al_2O_3-SiO_2-H_2O-CO_2 in the presence of quartz and magnetite were dicussed by Miyano and Klein (1989). Stilpnomelane is the most common Fe-bearing silicate in very low- to low-grade metamorphosed iron formations, and accommodates nearly all of the potassium in these systems. Stilpnomelane is estimated to be stable to ~430–470°C and 5–6 kbar, and will decompose to biotite and almandine at high temperature and to zussmanite and chlorite at higher pressure (Miyano & Klein, 1989). The hydrothermal ore deposit system, in which meifuite is found, has a similar mineral assemblage to that found in metamorphic iron formations (ferrous phyllosilicate + siderite + magnetite + quartz), indicating similar chemistry. Meifuite is also the only K-bearing mineral in the Al-deficient rock. The temperature/pressure condition should be well within the stability range of stilpnomelane (Miyano & Klein, 1989; Li et al., 2015). The major difference that might cause the crystallization of meifuite instead of stilpnomelane is the high activity of Cl, which is supported by the presence of hot saline fluids indicated by the fluid inclusions in the apatite next to meifuite crystals (Li et al., 2015).

If Cl is an important issue for the formation of meifuite, both Cl charge and size should be considered in the crystallization process. Concerning charge, in general, the O–H vector orientation in 2:1 trioctahedral phyllosilicates is perpendicular to the (001) plane (e.g. Giese, 1979) and the hydroxyl group proton acts on the interlayer cation to produce proton-cation repulsions. Studies of F substitution for (OH), where the proton is thereby eliminated and the attraction to cation is strengthened, show that this substitution greatly increases thermal stability, e.g. in phlogopite vs fluorophlogopite (e.g. Brigatti & Guggenheim, 2002). The substitution of Cl for OH is similar because of the charge relation and the elimination of the proton, and thus favors an increase in the meifuite thermal stability.

The structural control of the chlorine content of OH-bearing silicates was studied by Volfinger et al. (1985) who discovered that large octahedra/tetrahedra size ratio and more symmetrical hexagonal tetrahedral rings are essential to accommodate more Cl in the OH site. This is not a problem for ferrous phyllosilicates with large Fe-occupied octahedral sheets that stretch the tetrahedral sheet into near perfect hexagonal rings. The K atoms in the stilpnomelane structure are probably loosely bonded to the tetrahedral sheet without a well constrained site, which is indicated by the large space created by the double tetrahedra linkage between layers ($d_{001} \approx 12.2$ Å) (Eggleton & Bailey, 1964; Eggleton, 1972; Eggleton & Chappell, 1978; Guggenheim & Eggleton, 1987). The repulsion from the H atoms in the OH group would push the interlayer cations further away from the octahedral sheet, which is presumably why the extra space between layers is necessary to accommodate the alkaline elements at lower temperature and pressure. At higher temperatures, the H_2O molecules between layers would escape and the biotite structure become more stable; at higher pressures, the layers are pushed closer together, making the zussmanite structure more stable (Miyano & Klein, 1989). Replacing the OH group with Cl atoms on the octahedral sheet would remove the repulsion from H atoms and introduce an attraction force between O-sheet and the interlayer cations, making the accommodation of K or Na atoms with small d_{001} spacing possible, even at lower temperature and pressure than the condition required to stabilize biotite and zussmanite.

IMPLICATIONS

A new 2:1 (T–O–O–T) layer silicate with interlayer cations, meifuite, is recognized as belonging to the phyllosilicate group. Meifuite is the first strip structure of ferrous phyllosilicate to be discovered that can accommodate interlayer cations (K, Na) in specific interlayer sites. The other modulated 2:1 ferrous phyllosilicates, stilpnomelane and zussmanite, have island structures. The rare occurrence of the meifuite structure over the other ferrous phyllosilicates such as stilpnomelane suggests that special chemical conditions existed in the host rock. Strip structures of different width, combinations between similar structures such as meifuite and minnesotaite, or different polytypes might be expected in similar but slightly different geological environments. Future discovery and studies of these chemical and structural variations could provide more detailed information for a better understanding of these Fe-rich, low-grade metamorphic systems and hydrothermal systems.

SUPPLEMENTARY INFORMATION

The online version contains supplementary material available at https://doi.org/10.1007/s42860-021-00143-8.

ACKNOWLEDGMENTS

The authors are grateful to Prof. Xiang-Ping Gu from Central South University, who suggested this possible unknown phase. This study was supported partly by the Bailey Fellowship of the Department of Geoscience of the University of Wisconsin-Madison, the National Science Foundation (EAR-1530614), and a research grant from the National Natural Science Foundation of China (NSFC) (No.17306814).

Funding

Funding sources are as stated in the Acknowledgments.

Declarations

Conflict of Interest

The authors declare that they have no conflict of interest.

REFERENCES

Ahn, J. H., & Buseck, P. R. (1989). Microstructures and tetrahedral strip-width order and disorder in Fe-rich minnesotaites. *American Mineralogist, 74*, 384–393.

Blake, R. L. (1965). Iron phyllosilicates of the Cuyuna district in Minnesota. *American Mineralogist, 50*, 148–169.

Blöchl, P. E. (1994). Projector augmented-wave method. *Physical Review B, 50*, 17953–17979.

Brigatti, M.F. & Guggenheim, S. (2002). Mica crystal chemistry and the influence of pressure, temperature, and solid solution on atomistic models. Pp. 1–97 in: *Micas: Crystal Chemistry and Metamorphic Petrology* (A. Mottana, F.P. Sassi, and James B. Thompson, Jr, editors). *Reviews in Mineralogy and Geochemistry*, **46**, Mineralogical Society of America, Chantilly, VA, USA.

Brown, E. H. (1971). Phase relations of biotite and stilpnomelane in the greenschist facies. *Contributions to Mineralogy and Petrology, 31*, 275–299.

Eggleton, R. A. (1972). The crystal structure of stilpnomelane. Part II. The full cell. *Mineralogical Magazine, 38*, 693–711.

Eggleton, R. A., & Bailey, S. W. (1964). The crystal structure of stilpnomelane Part I. The Subcell. *Clays and Clay Minerals, 13*, 49–63.

Eggleton, R. A., & Chappell, B. W. (1978). The crystal structure of stilpnomelane. Part III: Chemistry and physical properties. *Mineralogical Magazine, 42*, 361–368.

Eggleton, R. A., & Guggenheim, S. (1986). A re-examination of the structure of ganophyllite. *Mineralogical Magazine, 50*, 307–315.

Giese, R. F. (1979). Hydroxyl orientations in 2:1 phyllosilicates. *Clays and Clay Minerals, 27*, 213–223.

Guggenheim, S., & Bailey, S. W. (1982). The superlattice of minnesotaite. *The Canadian Mineralogist, 20*, 579–584.

Guggenheim, S., & Eggleton, R. A. (1986a). Cation exchange in ganophyllite. *Mineralogical Magazine, 50*, 517–520.

Guggenheim, S., & Eggleton, R. A. (1986b). Structural modulations in iron-rich and magnesium-rich minnesotaite. *The Canadian Mineralogist, 24*, 479–497.

Guggenheim, S., & Eggleton, R. A. (1987). Modulated 2:1 layer silicates: review, systematics, and predictions. *American Mineralogist, 72*, 724–738.

Guggenheim, S., & Eggleton, R. A. (1994). A comparison of the structures and geometric stabilities of stilpnomelane and parsettensite: A distance least-squares (DLS) study. *American Mineralogist, 79*, 438–442.

Guggenheim, S., & Eggleton, R. A. (1998). Modulated crystal structures of greenalite and caryopilite: A system with long-range, in-plane structural disorder in the tetrahedra sheet. *The Canadian Mineralogist, 36*, 163–179.

Hazen, R. M., & Burnham, C. W. (1973). The crystal structures of one-layer phlogopite and annite. *American Mineralogist, 58*, 889–900.

Jefferson, D. A. (1976). Stacking disorder and polytypism in zussmanite. *American Mineralogist, 61*, 470–483.

Jin, S., Li, X., & Xu, H. (2020). Meifuite, IMA 2019-101. CNMNC Newsletter No. 54. *Mineralogical Magazine, 84*. https://doi.org/10.1180/mgm.2020.21

Jin, S., Xu, H., Lee, S., & Fu, P. (2018). Jinshajiangite: structure, twinning and pseudo-symmetry. *Acta Crystallographica Section B, 74*, 325–336.

Klein, C. (1974). Greenalite, stilpnomelane, minnesotaite, crocidolite and carbonates in a very low-grade metamorphic Precambrian iron formation. *The Canadian Mineralogist, 12*, 475–498.

Kresse, G., & Furthmülller, J. (1996). Efficient iterative schemes for ab initio total-energy calculations using a plane-wave basis set. *Physical Review B, 54*, 11169–11186.

Kresse, G., & Joubert, D. (1999). From ultrasoft pseudopotentials to the projector augmented-wave method. *Physical Review B, 59*, 1758–1775.

Leissner, L. (2014). Crystal chemistry of amphiboles studied by Raman spectroscopy. Mineralogisch-Petrographisches Institut-Universität Hamburg, Hamburg, Germany, 45 pp.

Li, X., Zhao, X., Zhou, M.-F., Chen, W. T., & Cho, Z. (2015). Fluid Inclusion and Isotopic Constraints on the Origin of the Paleoproterozoic Yinachang Fe-Cu-(REE) Deposit, Southwest China. *Economic Geology, 110*, 1339–1369.

Loewenstein, W. (1954). The distribution of aluminum in the tetrahedra of silicates and aluminates. *American Mineralogist, 39*, 92–96.

Lopes-Vieira, A., & Zussman, J. (1969). Further detail on the crystal structure of zussmanite. *Mineralogical Magazine, 37*, 49–60.

Miyano, T. (1982). Stilpnomelane, iron-rich mica, K-feldspar and hornblende in banded iron-formation assemblages of the Dales Gorge Member, Hamersley Group, Western Australia. *The Canadian Mineralogist, 20*, 189–202.

Miyano, T., & Klein, C. (1989). Phase equilibria in the system K_2O-FeO-MgO-Al_2O_3-SiO_2-H_2O-CO_2 and the stability limit of stilpnomelane in metamorphosed Precambrian iron-formations. *Contributions to Mineralogy and Petrology, 102*, 478–491.

Momma, K., & Izumi, F. (2011). VESTA 3 for three-dimensional visualization of crystal, volumetric and morphology data. *Journal of Applied Crystallography, 44*, 1272–1276.

Perdew, J. P., Burke, K., & Ernzerhof, M. (1996). Generalized gradient approximation made simple. *Physical Review Letters, 77*, 3865–3868.

Petříček, V., Dušek, M., & Palatinus, L. (2014). Crystallographic computing system JANA2006: General features. *Zeitschrift für Kristallographie-Crystalline Materials, 229*, 345–352.

Volfinger, M., Robert, J.-L., Vielzeuf, D., & Neiva, A. M. R. (1985). Structural control of the chlorine content of OH-bearing silicates (micas and amphiboles). *Geochimica et Cosmochimica Acta, 49*, 37–48.

Wang, L., Maxisch, T., & Ceder, G. (2006). Oxidation energies of transition metal oxides within the GGA+U framework. *Physical Review B, 73*, 195107.

Wang, A., Freeman, J. J., & Jolliff, B. L. (2015). Understanding the Raman spectral features of phyllosilicates. *Journal of Raman Spectroscopy, 46*, 829–845.

(Received 7 May 2021; revised 21 June 2021; AE: Warren D. Huff)